



Article

# Simulation and Optimization of a Hybrid Photovoltaic/Li-Ion Battery System

Xiaoxiao Yu <sup>1,2,3</sup>, Juntao Fan <sup>1</sup>, Zihua Wu <sup>1,2,3,\*</sup> , Haiping Hong <sup>1,\*</sup> , Huaqing Xie <sup>1,2,3</sup>, Lan Dong <sup>1,2,3</sup> and Yihuai Li <sup>1,2,3</sup>

<sup>1</sup> School of Energy and Materials, Shanghai Polytechnic University, Shanghai 201209, China; yuxx@sspu.edu.cn (X.Y.); 20221516118@stu.sspu.edu.cn (J.F.); hqxie@sspu.edu.cn (H.X.); donglan@sspu.edu.cn (L.D.); yhli@sspu.edu.cn (Y.L.)

<sup>2</sup> Shanghai Engineering Research Center of Advanced Thermal Functional Materials, Shanghai 201209, China

<sup>3</sup> Shanghai Thermophysical Properties Big Data Professional Technical Service Platform, Shanghai Polytechnic University, Shanghai 201209, China

\* Correspondence: wuzihua@sspu.edu.cn (Z.W.); hphong@sspu.edu.cn (H.H.)

**Abstract:** The coupling of solar cells and Li-ion batteries is an efficient method of energy storage, but solar power suffers from the disadvantages of randomness, intermittency and fluctuation, which cause the low conversion efficiency from solar energy into electric energy. In this paper, a circuit model for the coupling system with PV cells and a charge controller for a Li-ion battery is presented in the MATLAB/Simulink environment. A new three-stage charging strategy is proposed to explore the changing performance of the Li-ion battery, comprising constant-current charging, maximum power point tracker (MPPT) charging and constant-voltage charging stages, among which the MPPT charging stage can achieve the fastest maximum power point (MPP) capture and, therefore, improve battery charging efficiency. Furthermore, the charge controller can improve the lifetime of the battery through the constant-current and constant-voltage charging scheme. The simulation results indicate that the three-stage charging strategy can achieve an improvement in the maximum power tracking efficiency of 99.9%, and the average charge controller efficiency can reach 96.25%, which is higher than that of commercial chargers. This work efficiently matches PV cells and Li-ion batteries to enhance solar energy storages, and provides a new optimization idea for hybrid PV/Li-ion systems.



**Citation:** Yu, X.; Fan, J.; Wu, Z.; Hong, H.; Xie, H.; Dong, L.; Li, Y. Simulation and Optimization of a Hybrid Photovoltaic/Li-Ion Battery System. *Batteries* **2024**, *10*, 393. <https://doi.org/10.3390/batteries10110393>

Academic Editors: Rodolfo Dufo-López, Zhenbo Wang, Tingfeng Yi and Gang Sun

Received: 24 September 2024

Revised: 29 October 2024

Accepted: 5 November 2024

Published: 6 November 2024



**Copyright:** © 2024 by the authors. Licensee MDPI, Basel, Switzerland. This article is an open access article distributed under the terms and conditions of the Creative Commons Attribution (CC BY) license (<https://creativecommons.org/licenses/by/4.0/>).

## 1. Introduction

Currently, the world mainly uses non-renewable energy sources such as coal, oil, natural gas and nuclear energy. The use of non-renewable energy sources releases many gases and pollutants such as carbon dioxide, sulfur dioxide, etc., which cause serious environmental problems such as fog and frost, and land desertification and contribute to the greenhouse effect, while solar power generation is less harmful and more economic [1]. As a result, solar energy has been developed on a large scale as a renewable energy source, particularly photovoltaic (PV) power generation [2–4]. Recently, researchers have conducted extensive research on PV cells, for example, in material improvement, and have achieved the outstanding efficiency of ~23% [5–10]. However, weather conditions and round-the-clock changes affect the stability of PV cell power generation [11]. At present, coupled systems of PV cells and storage devices can reduce the impact from the environment; these include PV–battery systems and PV–phase-change material systems [12,13]. Among many solar energy utilization technologies, the combination of PV cells and batteries can transfer electric energy from PV cells into battery storage, and then the batteries generate electric energy to compensate for the lack of PV power generation caused by poor generation conditions [14,15]. Therefore, it is worth considering how to improve the match between PV cell and batteries.

Li-ion batteries have the advantages of cleanliness, light weight and high power density. Wang et al. [16] found that the charging time of  $\text{LiNi}_{0.8}\text{Mn}_{0.1}\text{Co}_{0.1}\text{O}_2$  (NMC811) || graphite lithium-ion batteries could be less than 15 mins, with a voltage higher than 4.5 V. Therefore, Li-ion batteries are considered as great electric energy storage devices and have been utilized for solar PV cell storages [17,18]. Guo et al. [19] proposed a three-stage charging control strategy based on a DC-DC converter to store solar energy in Li-ion batteries. These authors found that the improvement resulting from this strategy significantly enhanced the efficiency of converting solar energy into electrical energy. López et al. [20] utilized a simple MPPT method for a series DC-DC converter PV power system module to measure the PV cell generation voltage in real time and adjust the output power to keep the PV cells operating at maximum power. Bhan et al. [21] investigated the difference between charging systems with and without MPPT charging based on the MATLAB/Simulink environment, and found that a PV system with MPPT charging can generate more power. Szczepaniak et al. [22] proved that MPPT charging can improve generation efficiency. A coupling system combining a MPPT controller a PV generation system can enhance the stability of power generation, especially when the irradiation intensity changes [23,24]. However, the ability to adjust the PV maximum power point (MPP) voltage is still lacking, which reduces the conversion efficiency and shortens its lifetime [25]. Aljarhizi et al. [26] proposed a Li-ion battery charging method based on MPPT charging and a constant-voltage charging control, and found that the lifetime of a Li-ion battery can be extended without overloading. Even though the coupling of PV cells and a Li-ion battery with the MPPT charging method can improve the solar-to-electric efficiency and operating stability, the match of PV cells and Li-ion batteries still needs further optimization and improvement to ensure that the output current of PV cells at MPP meets the charging requirements of lithium-ion batteries; however, this issue is currently rarely studied.

This paper presents a model of a hybrid PV/Li-ion battery system in the MATLAB/Simulink environment. The new Li-ion battery charge controller utilizes an algorithm based on the combination of MPPT charging and Li-ion battery charging technology. The three-stage charging mode comprising constant-current charging, MPPT charging and constant-voltage charging, is utilized for improving the PV/Li-ion battery charging efficiency and effectively extending battery life.

## 2. System Modeling

Figure 1a shows the model diagram of the coupling system between PV cells and a Li-ion battery charge controller in the MATLAB/Simulink environment. It consists of a PV array, a DC-DC buck circuit, a Li-ion battery and a charge control module. Figure 1b illustrates that the charge control module comprises a Perturb and Observe (P&O) algorithm and a Li-ion battery charge control algorithm. The charge control module generates PWMs for switching the power switching tubes of the DC/DC buck circuit. The PV array module and Li-ion battery module are taken directly from the Simulink Simscape Electrical blockset library. The model uses a 2.7 kW PV array matched with a 12 V/10 Ah Li-ion battery. It was evaluated and simulated using MATLAB/Simulink. The circuitry model and charge controller block are explained in detail in the following sections.

### 2.1. DC-DC Buck Converter

As shown in Figure 1, a buck circuit is used in this design since it is more reliable and has less complexity [27–30]. The buck circuit comprises a MOSFET, a Schottky diode, an inductor, a resistor and two capacitors ( $C_1, C_2$ ). The switching frequency ( $f_s$ ) is equal to 1000 Hz. Equations (1)–(3) can be used to obtain the values of the buck circuit parameters L and C [31,32]. The capacitor  $C_1$  can stabilize the PV array's power output, and the value is set to 1  $\mu\text{F}$ . The value of the capacitor  $C_2$  is set to 625  $\mu\text{F}$ . The resistor R is a current-limiting resistor, and its parameter is set to 2  $\Omega$ . The forward voltage of the diode is set to 0.7 V.

$$D = \frac{U_o - 0.7}{U_i} \quad (1)$$

$$L = \frac{U_o * (1 - D)}{f_s * \Delta I_b} \quad (2)$$

$$C = \frac{U_i * (1 - D)}{8 * L * f_s * \Delta U_o} \quad (3)$$

where  $U_o$  represents the output voltage of the buck circuit,  $U_i$  represents the input DC voltage,  $\Delta I_b$  represents the ripple of the inductor current, and  $\Delta U_o$  represents the ripple in output voltage.

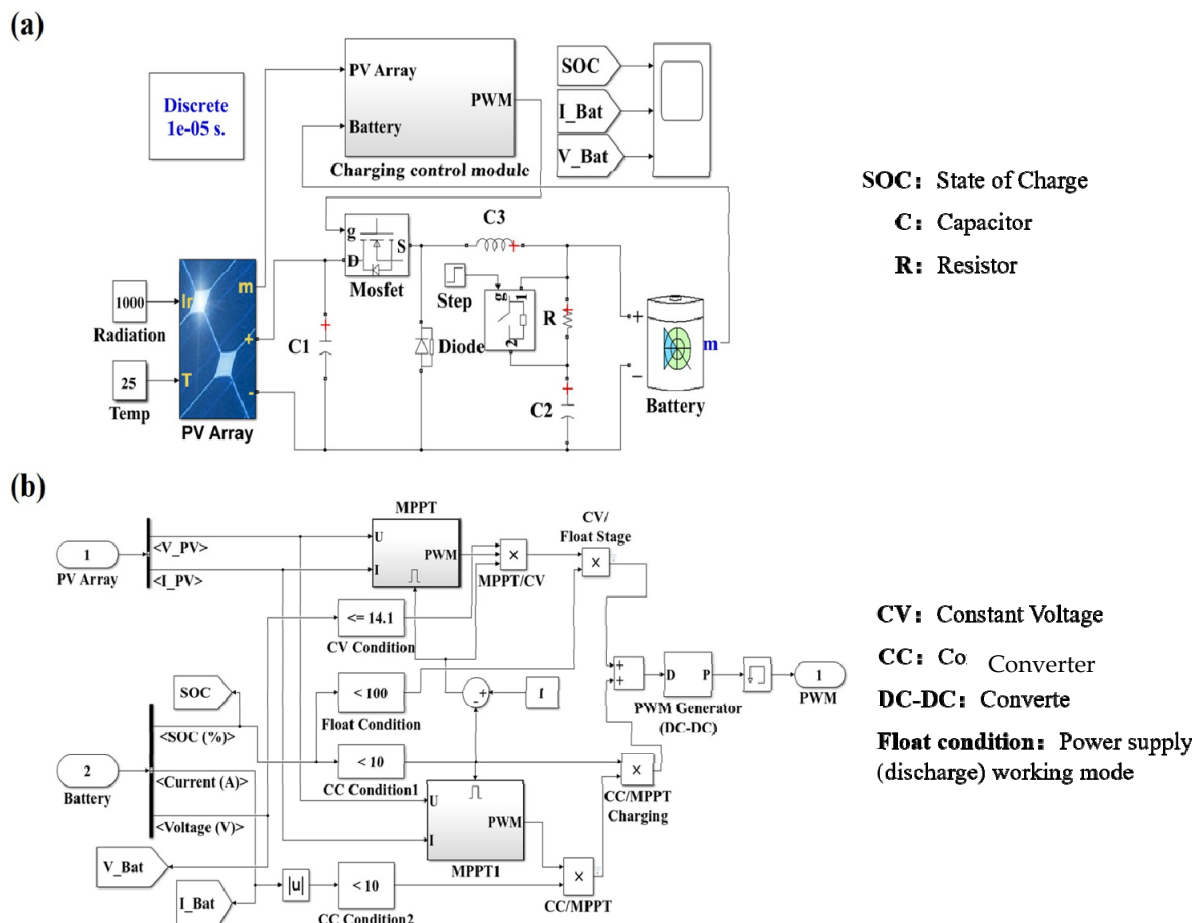


**Figure 1.** Charging control module: (a) solar PV/Li-ion battery charge controller module; (b) charge control algorithm module.

## 2.2. MPPT Algorithm

The power output from the PV panels changes as the irradiance value changes, and there is only one maximum power corresponding to each irradiance value. A model PV panel is simulated in the MATLAB/Simulink environment to analyze MPP, and its voltage-power (U-P) characteristic curves at different solar irradiance intensities are shown in Figure 2. It can be seen that the output power of the PV cell fluctuates with solar irradiance, and the MPP is the inflection point of the U-P curve, which indicates the highest generation power of the PV cells.

At present, the most commonly used MPPT algorithm is the Perturb and Observe (P&O) algorithm, and the flowchart of the P&O algorithm is shown in Figure 3a. The P&O algorithm is utilized to change the output power of PV cells through altering the equivalent load at the output of the cells and constantly adjusting the output power until the maximum output power [33–35]. Figure 3b is the flowchart of the P&O algorithm in the MATLAB/Simulink environment. It can be shown that the P&O algorithm is calculated through voltage  $U(k)$ , current  $I(k)$ , which is read from the PV array, and output power

$P(k)$ . Firstly, the unit delay block performs the previous sample ( $k - 1$ ) function. Then, the values of  $U(k) - U(k - 1)$  and  $P(k) - P(k - 1)$  are calculated by the unit delay block  $U(k - 1)$  and  $P(k - 1)$ . The signal module output 1 or  $-1$  determines the positive or negative state of the duty cycle. Of course, the duty cycle can be changed in steps of 0.01. The duty cycle signal is then connected to the buck section.

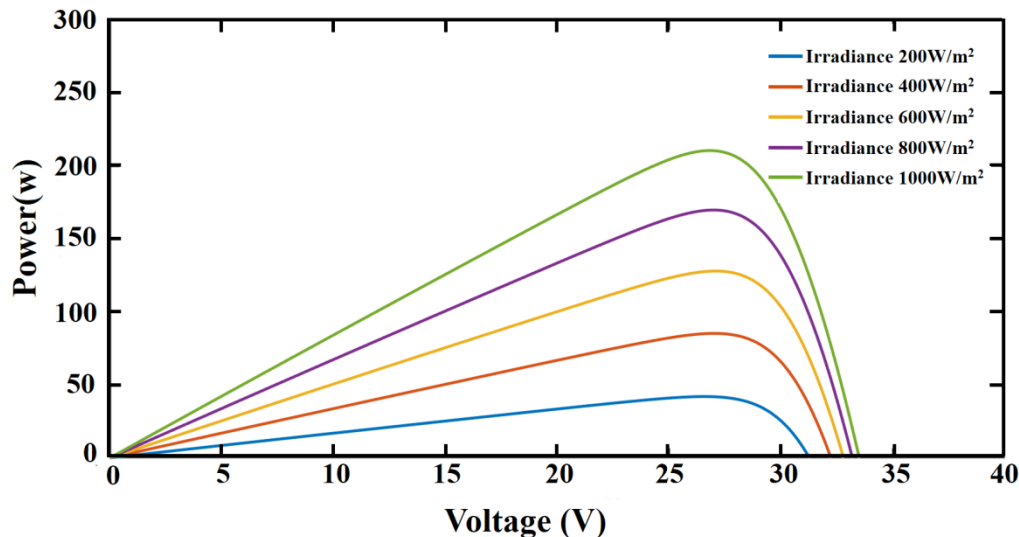


**Figure 2.** U-P characteristic curves of a solar cell.

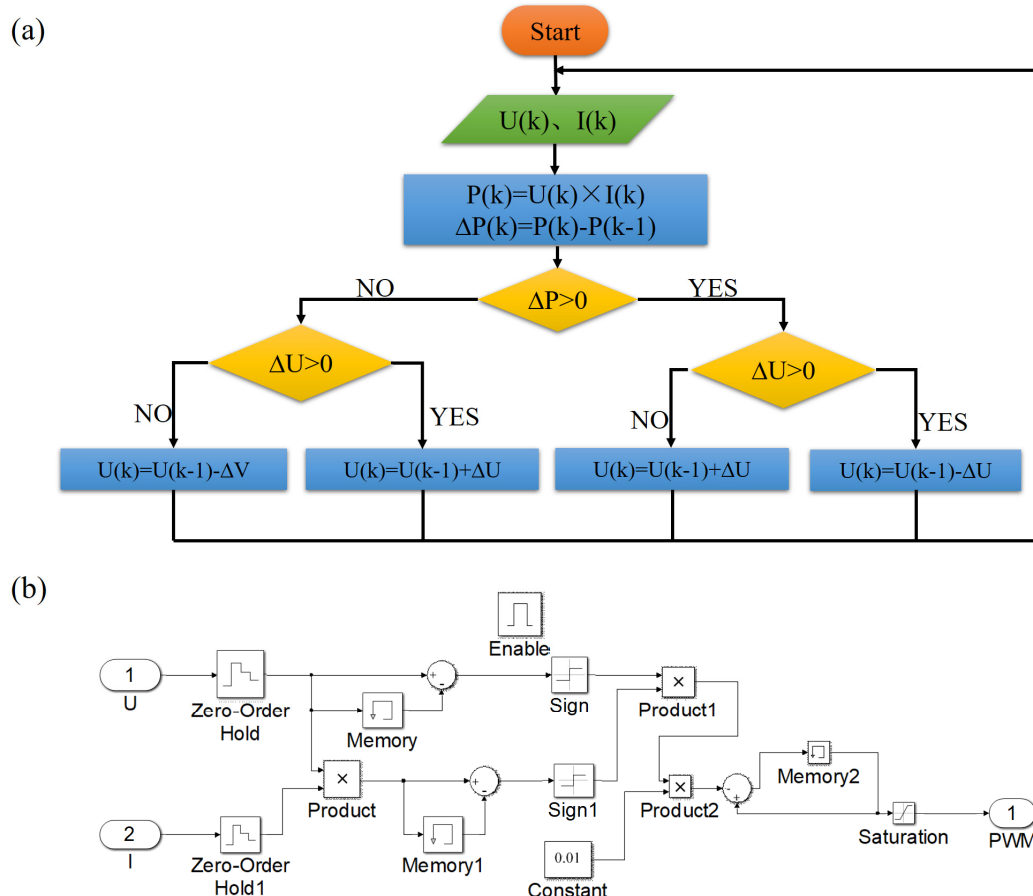


**Figure 3.** Implementation of the P&O algorithm. (a) Flowchart of the P&O algorithm. (b) P&O algorithm implementation in Simulink.

### 2.3. Li-Ion Battery Charging Control Method

Furthermore, the procedure of the Li-ion battery charging algorithm is shown in Figure 4. For  $\text{SoC} (\text{State of Charge}) \leq 10\%$ , the first stage maintains constant-current charging and MPPT charging, and the battery is charged at a constant current of 2 A (0.2 C). In particular, the charger switches to MPPT charging when the battery current is below the constant-current set value; otherwise, MPPT charging is prevented and the constant-current charging stage starts. For  $10\% < \text{SoC} \leq 95\%$ , the second stage enters MPPT charging, in which the battery is charged under a fluctuating current. Considering the effect of the weather on the output power of a PV array, it is important to match the models of the PV array and Li-ion battery to ensure that the MPPT charging current does not exceed the maximum charging current of the battery. Finally, for  $95\% < \text{SoC} \leq 100\%$ , the battery is charged at a constant voltage (14.1 V) during the third stage. The charger converts to MPPT charging if the battery voltage falls below the constant-voltage set value; otherwise, the constant-voltage charging continues.

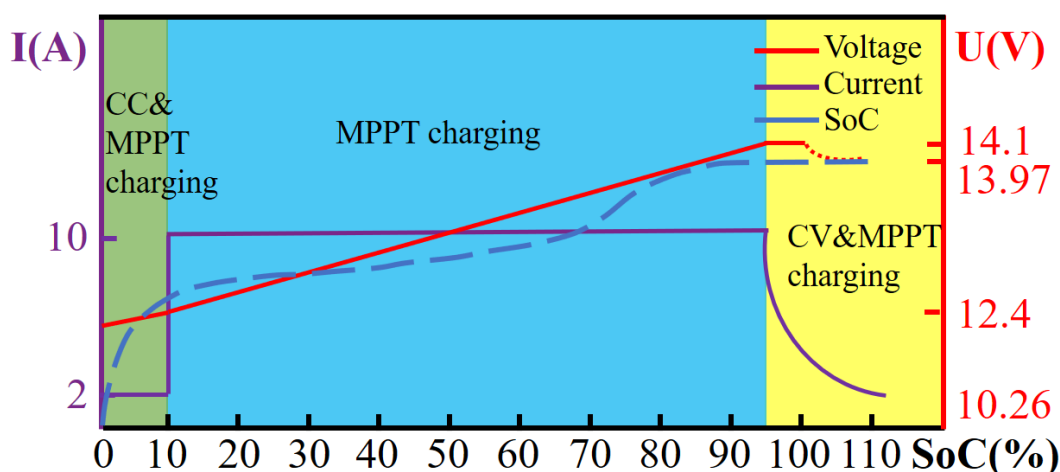


**Figure 4.** The charging process of the Li-ion battery.

### 3. Results and Discussion

In the MATLAB/Simulink environment, the PV–battery coupled system performance is simulated and examined. The discrete simulation type is established with a sample duration of  $10\ \mu\text{s}$  per sample, and the Simulink model is configured using automated solver selection with a variable step. This paper discusses the charging performance of Li-ion batteries, the tracking performance of MPPT, the overall efficiency performance, and the validation using conventional charge algorithms.

#### 3.1. Li-Ion Battery Charging Performance

The parameters of the PV array and Li-ion battery in the model are shown in Table 1. The PV array consists of four panels in series and produces 2.7 kW of power. The intensity of solar irradiation is set at  $1000\ \text{W/m}^2$ , the temperature is set to  $25\ ^\circ\text{C}$  and the time is set at 6000 s.

The charging process of the Li-ion battery is shown in Figure 5. It can be seen that the Li-ion battery is initially charged by the battery charge controller during the constant-current charging stage when SoC of the Li-ion battery is less than 10%. Furthermore, The MPPT charging stage begins when the battery SoC reaches 10% at 1800 s, and is maintained when the SoC reaches 95% at 4800 s. However, the MPPT charging is switched into the constant-voltage charging stage once the voltage of the Li-ion battery reaches 14.1 V. Moreover, SoC of the Li-ion battery at 5250 s reaches 100%, and then the charge controller switches to the float stage. Meanwhile, the Li-ion battery maintains a floating voltage of 14.0 V. Considering with the ideal charging process of Li-ion batteries reported in previous research [36], it is demonstrated that the Li-ion battery charging voltage and

current in this work meet the charge requirements as the current curve is almost identical to the ideal current curve.

**Table 1.** Parameters of photovoltaic arrays and Li-ion batteries.

	Parameters	Values
	Rated capacity	50 Ah
	Nominal voltage	12 V
	Full charge voltage	13.97 V
Li-ion battery	Constant-current charging current	10 A
	MPPT charging current	50 A
	Constant-voltage charging voltage	14.1 V
	Float charging voltage	13.97 V
	Maximum output power ( $P_{max}$ )	174 W
	Open circuit voltage ( $V_{oc}$ )	36.3 V
Solar panel	Maximum power point voltage ( $V_{mp}$ )	29 V
	Short-circuit current ( $I_{sc}$ )	6.5 A
	Maximum power point current ( $I_{mp}$ )	6 A

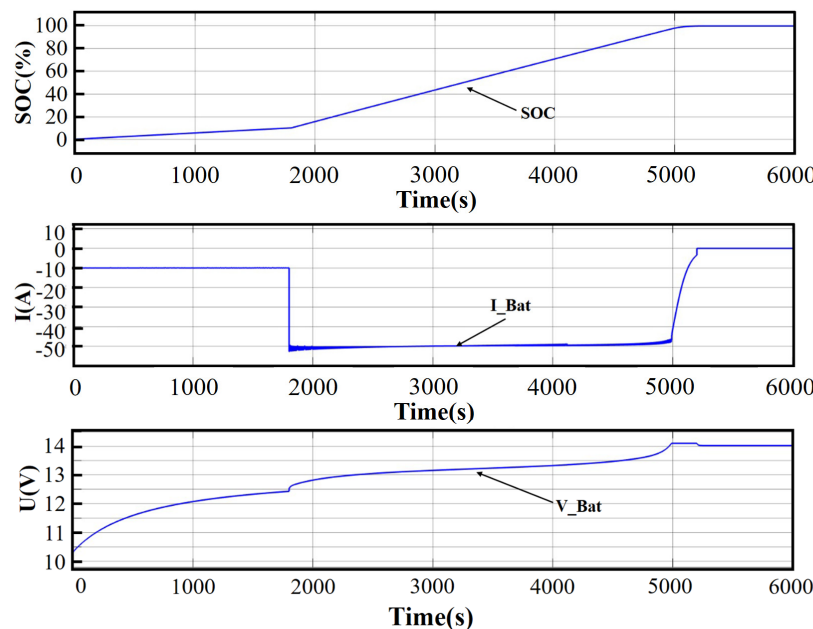


**Figure 5.** The process of the Li-ion battery charge.

### 3.2. MPPT Charging Efficiency

In this work, MPPT charging efficiency is defined by the ratio of the PV array output power to MPP power. Here, the effect of the solar irradiation intensity on the efficiency performance is further discussed. Considering the actual outdoor irradiation conditions, clouds affect the solar irradiation intensity, as shown in Figure 6a. In particular, the slower a cloud moves, the smaller the light intensity fluctuation is, and the better the tracking ability of the MPPT control method. Figure 6b clearly shows the efficiency and stability of the MPPT charging method, and the MPPT efficiency can reach 99.9% under the solar irradiation of 200–550 W/m<sup>2</sup>.

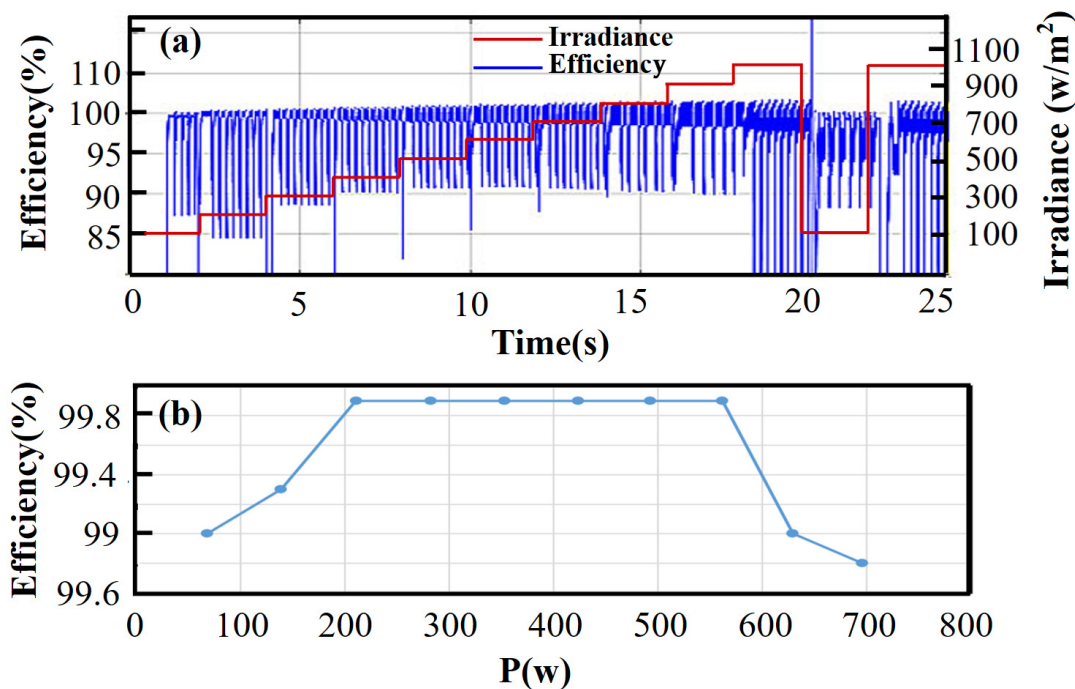


**Figure 6.** The performance analysis of MPPT charging. (a) Solar irradiance and MPPT charging real-time efficiency. (b) MPPT charging efficiency.

### 3.3. Overall Charging Efficiency of Li-Ions

Li-ion charger losses can drastically lower the overall efficiency of the energy storage. Here the overall efficiency of an Li-ion battery is defined by the ratio of the battery input power to the PV array output power. And the charging overall efficiencies of Li-ion batteries under three charging stages are discussed. According to Figure 7a, for  $0\% < \text{SoC} \leq 10\%$ , the constant-current charging efficiency can reach 95.5% at a solar irradiance of  $1000 \text{ W/m}^2$ . In addition, the MPPT charging efficiency can reach 95.5% at a solar irradiance of  $100 \text{ W/m}^2$ .

Aiming to highlight the characteristics of this work, the charging mode proposed in this paper and the traditional constant-current charging mode are compared through the same simulation method. Firstly, this study compares constant-current charging combined with MPPT charging to constant-current charging alone. The difference between the two charging methods in the early stage of charging are shown in Figure 7b,c. It can be seen that the two charge controllers have same charging performance under the constant-current charging stage. However, when the irradiation intensity decreases by  $100 \text{ W/m}^2$ , the three-stage charging mode can switch to the MPPT charging stage, and the charging efficiency can reach 0.25% at 60s, which is 0.7% SoC higher than the traditional charging mode.

For  $10\% < \text{SoC} \leq 95\%$ , the overall charging efficiency during the MPPT charging stage remains stable under uniform growth in the irradiation intensity, which indicates the MPPT method can efficiently achieve the maximum power charging. Moreover, the highest charging efficiency increases with the solar irradiation intensity, and reaches 97% when the irradiation intensity is  $1000 \text{ W/m}^2$ , as shown in Figure 8a. In particular, the MPPT charging method can rapidly resume a charging ability of 97% when the irradiation intensity undergoes large changes from  $100 \text{ W/m}^2$  to  $1000 \text{ W/m}^2$ .

Furthermore, the charging performance of the MPPT mode is compared with the constant-current charging mode in Figure 8b,c. It is easily seen that the MPPT charging mode results in a more stable charging state than the traditional mode when the irradiation intensity decreases from  $1000 \text{ W/m}^2$  to  $800 \text{ W/m}^2$ . Under the same charging time, the MPPT charging mode can achieve 11.6% SoC, which is 0.3% SoC higher than the constant-current charging mode alone.

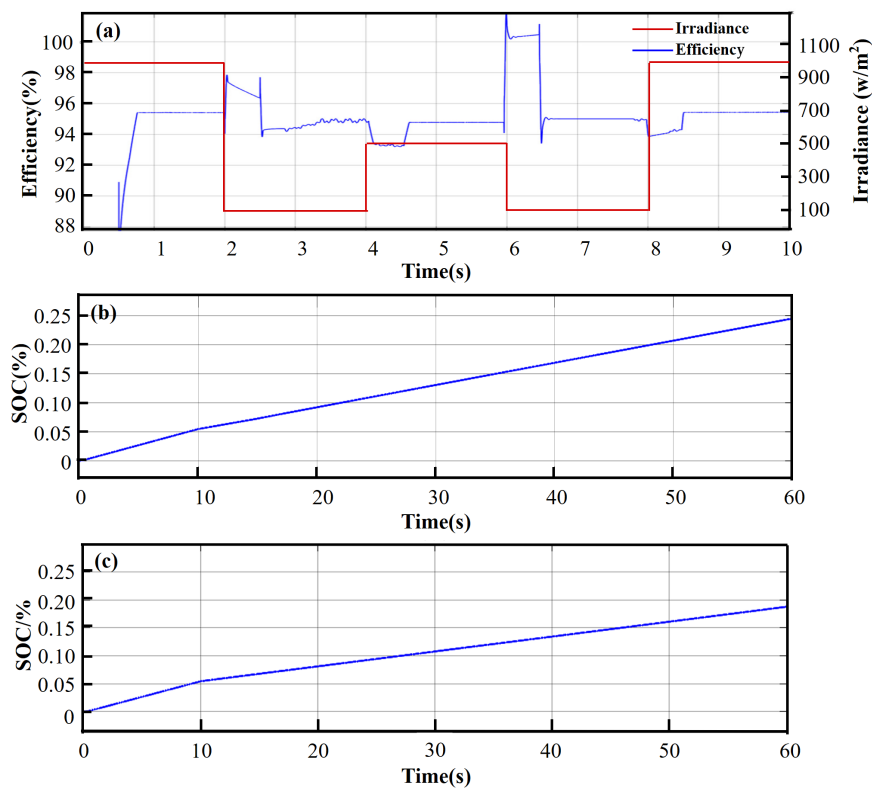


**Figure 7.** The overall performance analysis of the first-stage charging. (a) Solar irradiance and overall efficiency performance. (b) SoC variation with new charge controller. (c) SoC variation with traditional charge controller.

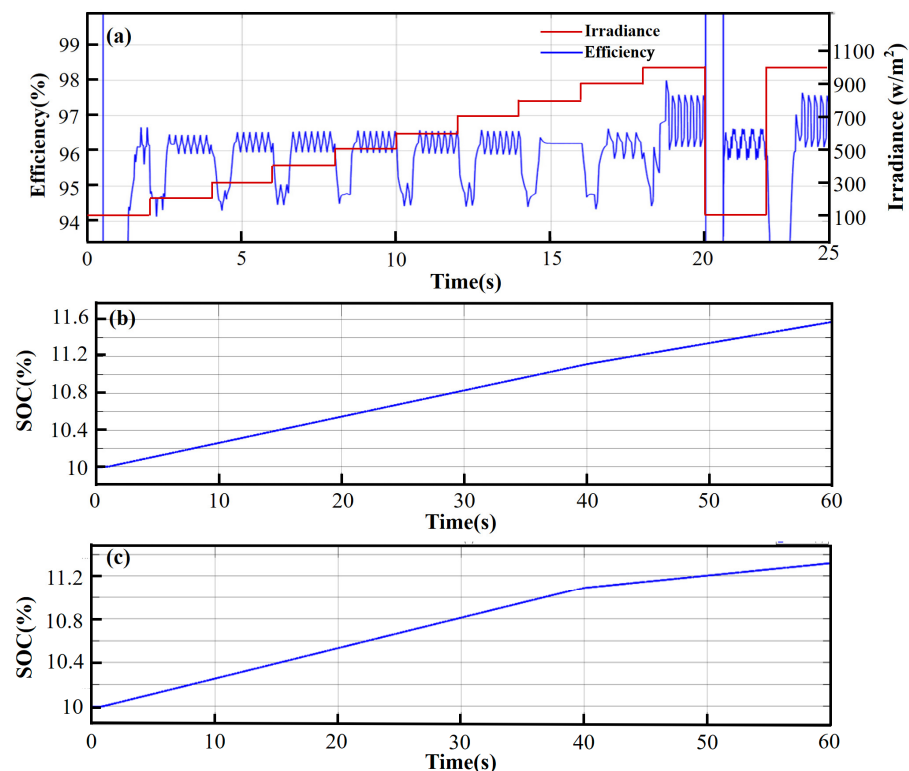


**Figure 8.** The overall performance analysis of the second-stage charging. (a) Light change process and overall conversion efficiency. (b) SoC variation with new charge controller. (c) SoC variation with traditional charge controller.

For  $95\% < \text{SoC} \leq 100\%$ , as illustrated in Figure 9a, from 0 to 2 s, the system is in constant-voltage charging mode, but the efficiency curve does not reach stability due to a delay in the simulation. From 2 to 4 s, the system switches to MPPT charging mode with an efficiency of approximately 97%. From 4 to 6 s, the system switches back to constant-voltage charging mode, with a charging efficiency of about 97%.

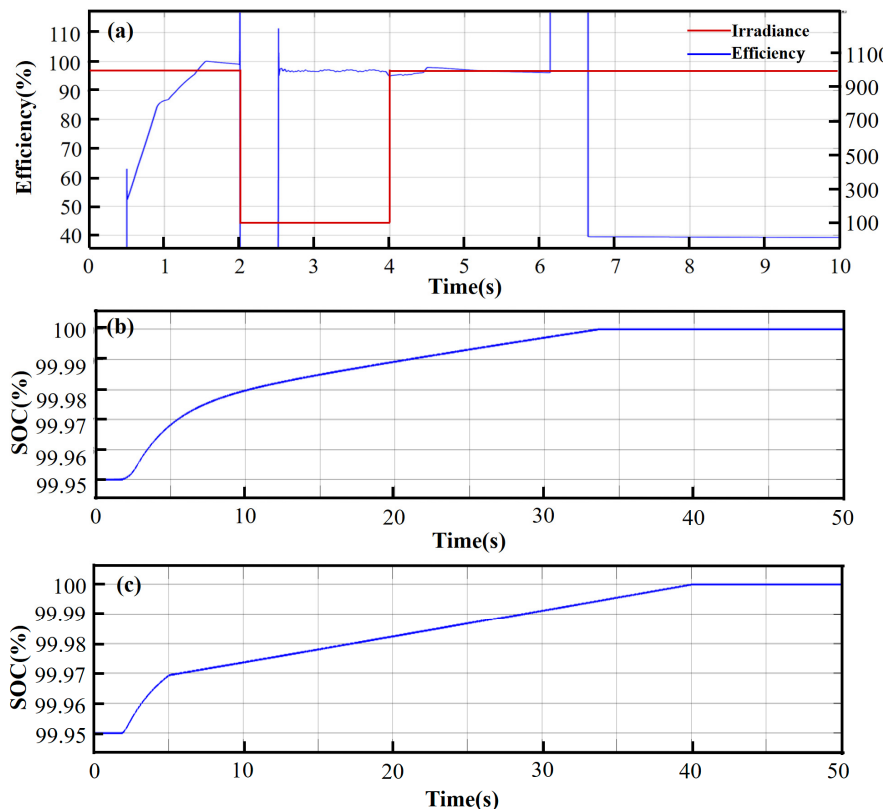


**Figure 9.** The overall performance analysis of the third-stage of charging. (a) Light change process and overall conversion efficiency. (b) SoC variation with new charge controller. (c) SoC variation with traditional charge controller.

Similarly, this study compares constant-voltage charging combined with MPPT charging to constant-voltage charging alone. Figure 9b,c show the difference between the two charging methods during the end stage of charging. Even though the two charging modes can achieve an SoC of 100%, the charging mode proposed in this work can decrease the charging time of the Li-ion battery to the maximum charging capacity by 5 s.

According to the above simulation results, the average conversion efficiency of the Li-ion battery charge controller is about 96.25%, with the highest efficiency of 97% and lowest efficiency of 95.5%. A comparison of the proposed system's charging efficiency with similar works already published is presented in Table 2.

**Table 2.** Recent research of nanofluid.

Ref.	System Efficiency
This work	95.5–97%
Palmiro et al. [37]	94–97%
López, J. [23]	85–95%
Zhang, L. [24]	87.48%
Salman et al. [34]	77.85–92.6%

In this section, the efficiency of the improved charging method is verified by comparison with the constant-current and constant-voltage charging methods. For  $10\% < \text{SOC} \leq 90\%$ , MPPT charging is more effective than constant-current charging. Combining constant-current charging and constant-voltage charging with MPPT charging can increase the charging power for Li-ion batteries in environments with varying solar irradiance. This offers faster charging speeds and higher charging efficiencies than charging with constant-current charging only or constant-voltage charging only.

#### 4. Conclusions

An efficient and safe charger system comprising PV cells and Li-ion batteries is crucial for solar energy storage and utilization. This work built a Li-ion battery charge controller model with the MPPT technique in the MATLAB/Simulink environment to explore the charging performance under an unstable surrounding environment. The charging method of the Li-ion battery, the buck circuit, and the maximum power tracking algorithm are all clearly analyzed. The results show that the three-stage charging mode utilized in this work can efficiently enhance battery charging efficiency due to the fastest MPP capture. Meanwhile, the Li-ion battery lifetime is significantly improved. In particular, the three-stage charging method has an average charge controller efficiency of 96.25%. It also shows a higher overall efficiency of 95.5–97% and shorter charging times than the traditional constant-current charging method. The improved charging techniques proposed by this work can enhance solar-driven PV cells–Li-ion battery charging control system performance and offer valuable experiences for further study.

**Author Contributions:** Conceptualization, Z.W.; methodology, X.Y. and J.F.; software, L.D.; validation, L.D.; formal analysis, L.D.; investigation, X.Y.; resources, Y.L.; data curation, Y.L.; writing—original draft preparation, X.Y. and J.F.; writing—review and editing, H.H.; supervision, Z.W. and H.X.; project administration, Z.W. All authors have read and agreed to the published version of the manuscript.

**Funding:** This work has been supported by research funding from the National Natural Science Foundation of China (No. 52176081), the Funding Programme Natural Science Foundation of Shanghai (No. 21ZR1424500), the Shanghai Local Capacity Building Programme (No. 22010500500 and No. 21010500700), the Shanghai Sailing Programme (No. 23YF1413500), the Shanghai Rising Star Programme (No. 21QA1403300) and the National Natural Science Foundation of China (No. 52306259).

**Data Availability Statement:** The original contributions presented in the study are included in the article.

**Acknowledgments:** We express our sincere gratitude to all those who contributed to this research; in particular, we thank Zihua Wu for his committed instruction and Xiaoxiao Yu for reviewing and editing the manuscript. We also appreciate the advice of Dong Lan, Yi-Huai, and Xie Hui-Qing. We also thank the two reviewers for their insightful and helpful criticism, which helped to strengthen the manuscript.

**Conflicts of Interest:** The authors declare no conflicts of interest.

#### References

1. Farghali, M.; Osman, A.I.; Mohamed, I.M.A.; Chen, Z.; Chen, L.; Ihara, I.; Yap, P.-S.; Rooney, D.W. Strategies to save energy in the context of the energy crisis: A review. *Environ. Chem. Lett.* **2023**, *21*, 2003–2039. [[CrossRef](#)] [[PubMed](#)]
2. Ranalder, L.; Gibb, D. *Renewables in Cities 2019 Global Status Report*; REN21: Paris, France, 2020; Volume 31.
3. Perez, M.; Perez, R. Update 2022—A fundamental look at supply side energy reserves for the planet. *Sol. Energy Adv.* **2022**, *2*, 100014. [[CrossRef](#)]
4. Djørup, S.; Thellufsen, J.Z.; Sorknæs, P. The electricity market in a renewable energy system. *Energy* **2018**, *162*, 148–157. [[CrossRef](#)]
5. Gao, Y.; Xiao, Z.; Cui, M.; Saidaminov, M.I.; Tan, F.; Shang, L.; Li, W.; Qin, C.; Ding, L. Asymmetric II-Bridge Engineering Enables High-Permittivity Benzo [1,2-B:4,5-b'] Difuran-Conjugated Polymer for Efficient Organic Solar Cells. *Adv. Mater.* **2024**, *36*, 2306373. [[CrossRef](#)]
6. Qi, X.; Song, C.; Zhang, W.; Shi, Y.; Gao, Y.; Liu, H.; Chen, R.; Shang, L.; Tan, H.; Tan, F.; et al. Bidirectional Targeted Therapy Enables Efficient, Stable, and Eco-Friendly Perovskite Solar Cells. *Adv. Funct. Mater.* **2023**, *33*, 2214714. [[CrossRef](#)]

7. Gao, Y.; Cui, M.; Qu, S.; Zhao, H.; Shen, Z.; Tan, F.; Dong, Y.; Qin, C.; Wang, Z.; Zhang, W.; et al. Efficient Organic Solar Cells Enabled by Simple Non-Fused Electron Donors with Low Synthetic Complexity. *Small* **2022**, *18*, 2104623. [[CrossRef](#)]
8. Huang, X.; Gao, Y.; Li, W.; Wang, J.; Yue, G.; Tan, F.; Wang, H.L. Efficient and Stable Z907-Based Dye-Sensitized Solar Cells Enabled by Suppressed Charge Recombination and Photocatalytic Activity. *ACS Sustain. Chem. Eng.* **2024**, *12*, 13007–13016. [[CrossRef](#)]
9. He, S.; Lan, Z.; Zhang, B.; Gao, Y.; Shang, L.; Yue, G.; Chen, S.; Shen, Z.; Tan, F.; Wu, J. Holistically Optimizing Charge Carrier Dynamics Enables High-Performance Dye-Sensitized Solar Cells and Photodetectors. *ACS Appl. Mater. Interfaces* **2022**, *14*, 43576–43585. [[CrossRef](#)]
10. Gao, Y.; Shen, Z.; Tan, F.; Yue, G.; Liu, R.; Wang, Z.; Qu, S.; Wang, Z.; Zhang, W. Novel benzo [1,2-b:4,5-b'] difuran-based copolymer enables efficient polymer solar cells with small energy loss and high VOC. *Nano Energy* **2020**, *76*, 104964. [[CrossRef](#)]
11. Dubey, S.; Sarvaiya, J.N.; Seshadri, B. Temperature Dependent Photovoltaic (PV) Efficiency and Its Effect on PV Production in the World—A Review. *Energy Procedia* **2013**, *33*, 311–321. [[CrossRef](#)]
12. Koutroulis, E.; Kalaitzakis, K. Novel battery charging regulation system for photovoltaic applications. *IEE Proc. Electr. Power Appl.* **2004**, *151*, 191–197. [[CrossRef](#)]
13. Stropnik, R. Increasing the efficiency of PV panel with the use of PCM. *Renew. Energy* **2016**, *97*, 671–679. [[CrossRef](#)]
14. Dunn, B.; Kamath, H.; Tarascon, J.-M. Electrical Energy Storage for the Grid: A Battery of Choices. *Science* **2011**, *334*, 928–935. [[CrossRef](#)] [[PubMed](#)]
15. Maheswari, L.; Sornavadi, R.; Vijayalakshmi, S. Modeling and Simulation of Buck Converter for Charging Battery by Solar Photovoltaic System. *Appl. Mech. Mater.* **2014**, *592*, 2379–2385. [[CrossRef](#)]
16. Xu, J.; Zhang, J.; Pollard, T.P.; Li, Q.; Tan, S.; Hou, S.; Wang, C. Electrolyte design for Li-ion batteries under extreme operating conditions. *Nature* **2023**, *614*, 694–700. [[CrossRef](#)] [[PubMed](#)]
17. Kebede, A.A.; Coosemans, T.; Messagie, M.; Jemal, T.; Behabtu, H.A.; Van Mierlo, J.; Berecibar, M. Techno-economic analysis of lithium-ion and lead-acid batteries in stationary energy storage application. *J. Energy Storage* **2021**, *40*, 102748. [[CrossRef](#)]
18. Anuphappharadorn, S.; Sukchai, S.; Sirisamphanwong, C.; Ketjoy, N. Comparison the Economic Analysis of the Battery between Lithium-ion and Lead-acid in PV Stand-alone Application. *Energy Procedia* **2014**, *56*, 352–358. [[CrossRef](#)]
19. Guo, L.; Brewer, A.; Speiser, B. Design and Implementation of A Solar Battery Charger. In Proceedings of the 2010 Annual Conference & Exposition, Louisville, KY, USA, 20 June 2010.
20. López, J.; Seleme Jr, S.I.; Donoso, P.F.; Morais LM, F.; Cortizo, P.C.; Severo, M.A. Digital control strategy for a buck converter operating as a battery charger for stand-alone photovoltaic systems. *Sol. Energy* **2016**, *140*, 171–187. [[CrossRef](#)]
21. Bhan, V.; Shaikh, S.A.; Khand, Z.H.; Ahmed, T.; Khan, L.A.; Chachar, F.A.; Shaikh, A.M. Performance Evaluation of Perturb and Observe Algorithm for MPPT with Buck-Boost Charge Controller in Photovoltaic Systems. *J. Control Autom. Electr. Syst.* **2021**, *32*, 1652–1662. [[CrossRef](#)]
22. Szczepaniak, M.; Otreba, P.; Otreba, P.; Sikora, T. Use of the Maximum Power Point Tracking Method in a Portable Lithium-Ion Solar Battery Charger. *Energies* **2021**, *15*, 26. [[CrossRef](#)]
23. Anowar, M.H.; Roy, P. A Modified Incremental Conductance Based Photovoltaic MPPT Charge Controller. In Proceedings of the 2019 International Conference on Electrical, Computer and Communication Engineering (ECCE), Cox's Bazar, Bangladesh, 7–9 February 2019; IEEE: New York, NY, USA, 2019; pp. 1–5. [[CrossRef](#)]
24. Zhang, L.; Wang, Z.; Cao, P.; Zhang, S. A Maximum Power Point Tracking Algorithm of Load Current Maximization-Perturbation and Observation Method with Variable Step Size. *Symmetry* **2020**, *12*, 244. [[CrossRef](#)]
25. Gibson, T.L.; Kelly, N.A. Solar photovoltaic charging of lithium-ion batteries. *J. Power Sources* **2010**, *195*, 3928–3932. [[CrossRef](#)]
26. Aljarhizi, Y.; Hassouna, A.; Al Ibrahim, E.M. Control Management System of a Lithium-ion Battery Charger Based MPPT algorithm and Voltage Control. In Proceedings of the 2019 5th International Conference on Optimization and Applications (ICOA), Kenitra, Morocco, 25–26 April 2019; IEEE: New York, NY, USA, 2019; pp. 1–6. [[CrossRef](#)]
27. Mirzaei, A. Design and construction of a charge controller for stand-alone PV/battery hybrid system by using a new control strategy and power management. *Sol. Energy* **2017**, *149*, 132–144. [[CrossRef](#)]
28. Taghvaei, M.H.; Radzi, M.A.M.; Moosavain, S.M.; Hizam, H.; Marhaban, M.H. A current and future study on non-isolated DC-DC converters for photovoltaic applications. *Renew. Sustain. Energy Rev.* **2013**, *17*, 216–227. [[CrossRef](#)]
29. Coelho, R.F. Influence of Power Converters on PV Maximum Power Point Tracking Efficiency. In Proceedings of the 2012 10th IEEE/IAS International Conference on Industry Applications, Fortaleza, Brazil, 5–7 November 2012; IEEE: New York, NY, USA, 2012.
30. Venkatramanan, D.; John, V. Dynamic Modeling and Analysis of Buck Converter Based Solar PV Charge Controller for Improved MPPT Performance. *IEEE Trans. Ind. Appl.* **2019**, *55*, 6234–6246. [[CrossRef](#)]
31. Pathare, M.; Shetty, V.; Datta, D.; Valunjkar, R.; Sawant, A.; Pai, S. Designing and Implementation of Maximum Power Point Tracking(MPPT) Solar Charge Controller. In Proceedings of the 2017 International Conference on Nascent Technologies in Engineering, Navi Mumbai, India, 27–28 January 2017; p. 5.
32. Tan, R.H.; Er, C.K.; Solanki, S.G. Modeling of Photovoltaic MPPT Lead Acid Battery Charge Controller for Standalone System Applications. *E3S Web Conf.* **2020**, *182*, 03005. [[CrossRef](#)]

33. Kaur, T.; Gambhir, J.; Kumar, S. Arduino based solar powered battery charging system for rural SHS. In Proceedings of the 2016 7th India International Conference on Power Electronics (IICPE), Patiala, India, 17–19 November 2016; IEEE: New York, NY, USA, 2016; pp. 1–5. [[CrossRef](#)]
34. Salman, S.; Ai, X.; Wu, Z. Design of a P-&-O algorithm based MPPT charge controller for a stand-alone 200W PV system. *Prot. Control Mod. Power Syst.* **2018**, *3*, 25.
35. de Brito, M.A.G.; Galotto, L.; Sampaio, L.P.; e Melo, G.D.A.; Canesin, C.A. Evaluation of the Main MPPT Techniques for Photovoltaic Applications. *IEEE Trans. Ind. Electron.* **2013**, *60*, 1156–1167. [[CrossRef](#)]
36. Gao, Y.; Zhang, X.; Cheng, Q.; Guo, B.; Yang, J. Classification and Review of the Charging Strategies for Commercial Lithium-Ion Batteries. *IEEE Access* **2019**, *7*, 43511–43524. [[CrossRef](#)]
37. Palmiro, F.; Rayudu, R.; Ford, R. Modelling and simulation of a solar PV lithium ion battery charger for energy kiosks application. In Proceedings of the 2015 IEEE PES Asia-Pacific Power and Energy Engineering Conference (APPEEC), Brisbane, Australia, 15–18 November 2015; IEEE: New York, NY, USA, 2015; pp. 1–5. [[CrossRef](#)]

**Disclaimer/Publisher’s Note:** The statements, opinions and data contained in all publications are solely those of the individual author(s) and contributor(s) and not of MDPI and/or the editor(s). MDPI and/or the editor(s) disclaim responsibility for any injury to people or property resulting from any ideas, methods, instructions or products referred to in the content.